Quaternary Science Reviews 227 (2020) 106048

Contents lists available at ScienceDirect

Quaternary Science Reviews

journal homepage: www.elsevier.com/locate/quascirev

Possible link of an exceptionally strong East Asian summer monsoon to a La Niña-like condition during the interglacial MIS-13

Hao Lu [a, b], Qiuzhen Yin [b], Jia Jia [c, *], Dunsheng Xia [a], Fuyuan Gao [d], Anqi Lyu [b], Yapeng Ma [a], Fan Yang [a]

[a] Key Laboratory of West China's Environmental System (Ministry of Education), College of Earth and Environmental Sciences, Lanzhou University, Lanzhou 730000, China
[b] Georges Lemaître Centre for Earth and Climate Research, Earth and Life Institute, Université Catholique de Louvain, 1348 Louvain-La-Neuve, Belgium
[c] College of Geography and Environment Sciences, Zhejiang Normal University, Zhejiang 321004, China
[d] College of Geography and Environment Engineering, Lanzhou City University, 730070, China

ARTICLE INFO

Article history:
Received 27 March 2019
Received in revised form
5 November 2019
Accepted 5 November 2019
Available online 14 November 2019

Keywords:
Paleosol formation
Magnetic susceptibility
MIS-13
East Asian summer monsoon
Interglacial
Chinese Loess Plateau

ABSTRACT

Previous studies from the central and eastern Chinese Loess Plateau (CLP) showed that the S5-1 paleosol, which corresponding to Marine Isotope Stage (MIS) 13, was the strongest developed during the last million years, suggesting extremely strong East Asian summer monsoon (EASM). However, evidence shows that regional diversity exists in the relative intensity of the S5-1 soil formation. In this study, we first verify systematically the S5-1 soil development across the whole CLP by using numerous loess records. We then examine the spatial variation of the magnetic susceptibility of different loess-paleosol sections to identify the spatial change of the EASM intensity during MIS-13. We also compare the loess records with other monsoon records in China. Our results show that, in central CLP, S5-1 is indeed the strongest developed as suggested by previous studies, whereas in the western CLP, it is weakly developed and the S4 paleosol developed during MIS-11 is the strongest. As compared to MIS-11, the northern front of the EASM during MIS-13 didn't penetrate into western CLP, but was located more northerly and eastward. Based on sea surface temperature records in the tropical Pacific, we suggest that the temporal and spatial abnormal variation of the EASM during MIS-13 could be related to a strong La Niña or La Niña-like climate condition. Under such condition, the Western Pacific Subtropical High (WPSH) becomes weaker and retreats more northeastward, leading to more precipitation in the mid-east region of northern China but less rainfall in the western inland.

© 2019 Published by Elsevier Ltd.

1. Introduction

The East Asian summer monsoon (EASM) is generated by the heat contrast between the Pacific Ocean and the Asian landmass, and is further enhanced by the thermal and dynamic effects of the Tibetan Plateau. In the last two decades, numerous studies have focused on the EASM moisture source, drive forces and interdecadal variability (e.g. Zhou and Yu, 2005; Ding et al., 2018). The abnormal variability of the EASM can cause unbalanced distribution of summer precipitation and result in severe droughts or floods that have devastating effects on society in densely populated East Asia (e.g. Webster et al., 1998). Thus it is important to investigate the variability of the EASM on various time-scales and to explore its underlying forcing mechanisms, in order to improve our ability to predict the long-term trends of regional and global climate in the context of global warming.

Marine isotope stage 13 (MIS-13), an interglacial about 500 ka years ago, is a special and controversial stage of paleoclimatic evolution. It is characterized by a relatively lower CO_2 concentrations (Lüthi et al., 2008) (Fig. 1c), cooler Antarctic temperatures (Jouzel et al., 2007) (Fig. 1d) and high benthic $\delta^{18}O$ values (e.g., Lisiecki and Raymo, 2005) (Fig. 1a), indicating that MIS-13 is a relatively cool interglacial in comparison with other interglacials of the past 800 ka. However, the paleosol S5-1, corresponding to MIS-13, from the central Chinese Loess Plateau (CLP), had undergone the most intense pedogenesis and represented the moistest environment of the past 800 ka, suggesting extremely strong EASM (e.g. Kukla et al., 1990; Guo et al., 1998) (Fig. 1b). This climatic event is

* Corresponding author.
E-mail address: jiaj@zjnu.edu.cn (J. Jia).

https://doi.org/10.1016/j.quascirev.2019.106048
0277-3791/© 2019 Published by Elsevier Ltd.

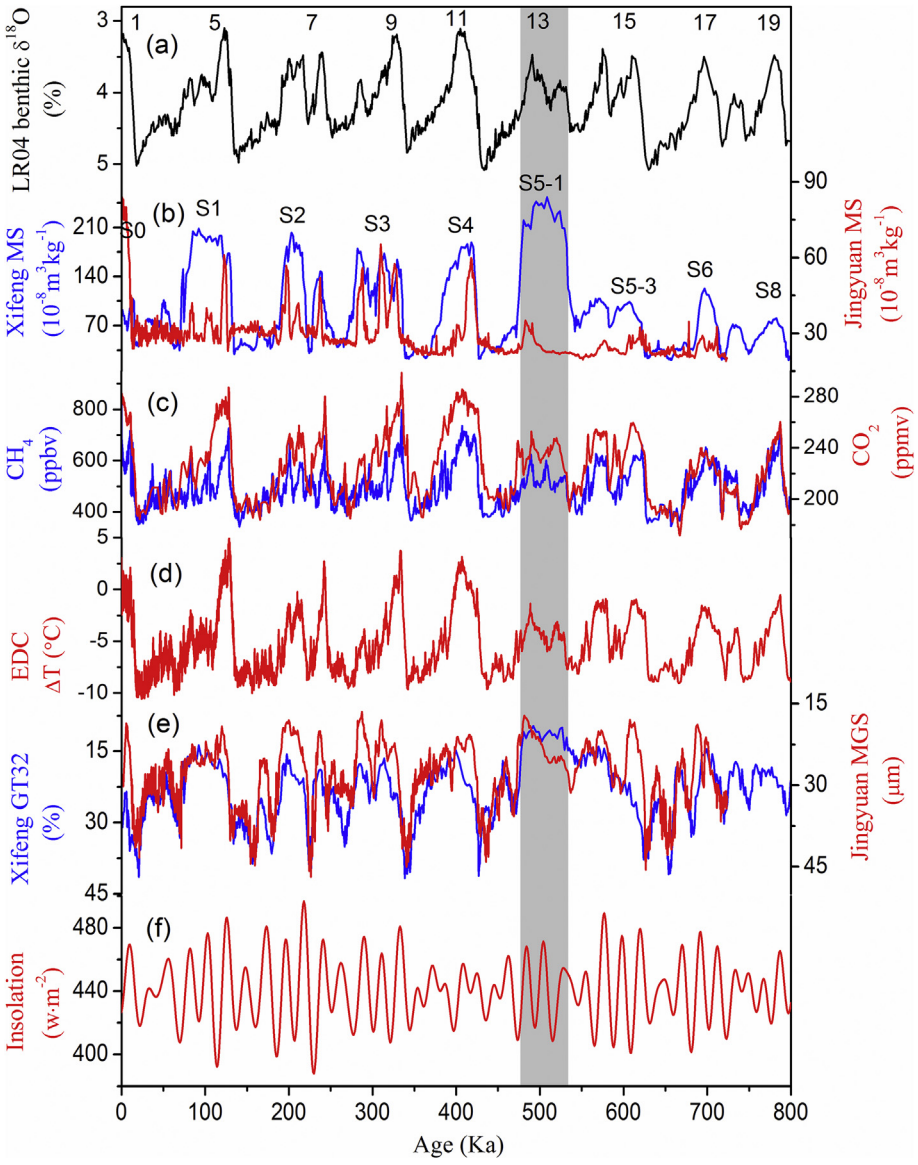

Fig. 1. Comparison of the China loess proxies of East Asian monsoon with relevant ice, marine records and insolation. (a) Marine $\delta^{18}O$ record (black) (Lisiecki and Raymo, 2005) with the interglacials oxygen isotope stages (MIS) labelled at the top part; (b) loess magnetic susceptibility at Xifeng (blue) (Guo et al., 2009) and Jingyuan (red) (Sun et al., 2006a) with the major paleosol units labelled; (c) Antarctic CH_4 (blue) (Loulergue et al., 2008) and CO_2 records (red) (Lüthi et al., 2008); (d) EDC ΔT record (red) (Jouzel et al., 2007); (e) loess grain size GT32 (>32 μm %) and MGS (mean grain size) at Xifeng (blue) (Guo et al., 2009), Jingyuan (red) (Sun et al., 2006a); (f) July insolation 65° N (Berger and Loutre, 1991). Gray frame denote the proxies for which MIS-13 can be considered as typical from an amplitude signal point of view. (For interpretation of the references to color in this figure legend, the reader is referred to the Web version of this article.)

not isolated, strong African and Indian monsoons during MIS-13 were also suggested based on marine sediments from the equatorial Indian Ocean (Bassinot et al., 1994) and the Mediterranean Sea (Rossignol-Strick et al., 1998). The corresponding paleosol of the Serbian loess in the Southeastern European is also shown to be the most developed (Bronger, 2003; Buggle et al., 2009; Marković et al., 2009, 2012, 2015). While soil micromorphology, magnetic parameters and redness indicate the paleosol S5-1 unit of Tajikistan loess in central Asia is relatively weak (Bronger et al., 1998; Ding et al., 2002; Jia et al., 2018a). A strong EASM occurring during a relatively cool interglacial MIS-13 was pointed out by Yin and Guo (2008) as a seeming paradox in that the CO_2 and CH_4 concentrations were relatively low and its insolation is not abnormal as compared to other interglacials (Fig. 1c and f). In order to understand this seeming paradox, different proposals have been made to explain the strong summer monsoon during MIS-13, for example, hemisphere climate asymmetry (Guo et al., 2009). Climate models of different complexities have also been used to investigate the response of the EASM to insolation, greenhouse gases concentration, ice sheets, the size of Tibetan Plateau and the tropical Pacific surface condition (Yin et al., 2008, 2009, 2014; Muri et al., 2012; Sundaram et al., 2012; Karami et al., 2015). However, the climatic paradox question remains open to solve, possibly and at least partly due to uncertainties in climate models and/or inaccurate experiment set up. The recent study suggests that the extremely high MS of the S5-1 paleosol in the central CLP is mainly attributed to extremely humid environment (Lu et al., 2018) rather than long duration of pedogenic weathering (Bronger, 2003; Finke et al., 2017) due to anomalously low loess deposition rate, confirming a strong EASM during MIS-13.

In the meantime, regional diversity might exist in the relative intensity of the S5-1 soil formation. Specifically, different from the S5-1 paleosol in the central and eastern CLP, the magnetic susceptibility (MS) of S5-1 in the Jingyuan section, which is located in the northwestern CLP, is obviously lower than that of the overlying paleosol layers (Fig. 1b), indicating weaker paleosol development (Sun et al., 2006a). This regional discrepancy may signify that the strong EASM during MIS-13 brings less rainfall to the western CLP, resulting in weaker soil development there. This is another paradox, because a strong EASM could have brought a large amount of rainfall and strongly affected the western CLP. However, due to lack of comparative study of climatic records between the CLP and the other EASM regions, study of the spatial change of the EASM intensity during MIS-13 is rare and the mechanism of the two paradoxes mentioned above remains to be understood.

Previous studies focused only on a few loess sites located in the central and eastern CLP (e.g. Yin and Guo, 2008; Guo et al., 2009). Here we first verify the S5-1 soil development condition by systematically compiling as many as possible the loess records of the S5-1 paleosol across the whole CLP including both the central-eastern CLP and the western CLP. We also examine the spatial variation of MS of different loess-paleosol sections to identify the spatial change of the EASM intensity in the CLP during MIS-13 and compare it with MIS-11. Finally, we compare the loess records with records from other regions of monsoonal China and discuss about the mechanism of these paradoxes.

2. General setting and methods

The CLP is located in the summer monsoon boundary zone in northern China, extending over 3.8×10^5 km^2, from the southern margin of Mongolia and eastern margin of Tibet Plateau thence south and east to the Taihang Mountains and Qinling Mountains (Fig. 2a). It is divided into three geographical sub-regions by the Liupan Mountains and the Lvliang Mountains: the western, the central and the eastern CLP (Liu, 1985) (Fig. 2b). The modern climate of the CLP is characterized by seasonal alternations of a wet, warm summer monsoon and a dry, cold winter monsoon. The main sources of moisture for the CLP in summer originate from adjacent Oceans (e.g. the Bay of Bengal, the South China Sea, the Arabian Sea) (Hu et al., 2016). The average annual rainfall and temperature decreases from ~700 mm to ~300 mm and ~13 °C to ~7 °C, from southeast to northwest, with ~60–80% of the precipitation concentrating in summer season. The degree of the paleosol development is linked strongly to variations in precipitation and has been widely accepted as a reliable signal of EASM intensity (Zhou et al., 1996; Chen et al., 1997; An, 2000; Sun et al., 2006a). A stronger EASM transports more heat and moisture to the middle-high latitude regions (An et al., 2000; Ding et al., 2001a), resulting in stronger chemical weathering and paleosol development. Conversely, when the EASM gets weaker, the pedogenesis in the loess deposit is diminished resulting from reduced chemical weathering and increased loess accumulation rate (Chen et al., 2000). Therefore, the EASM intensity can be reflected by the

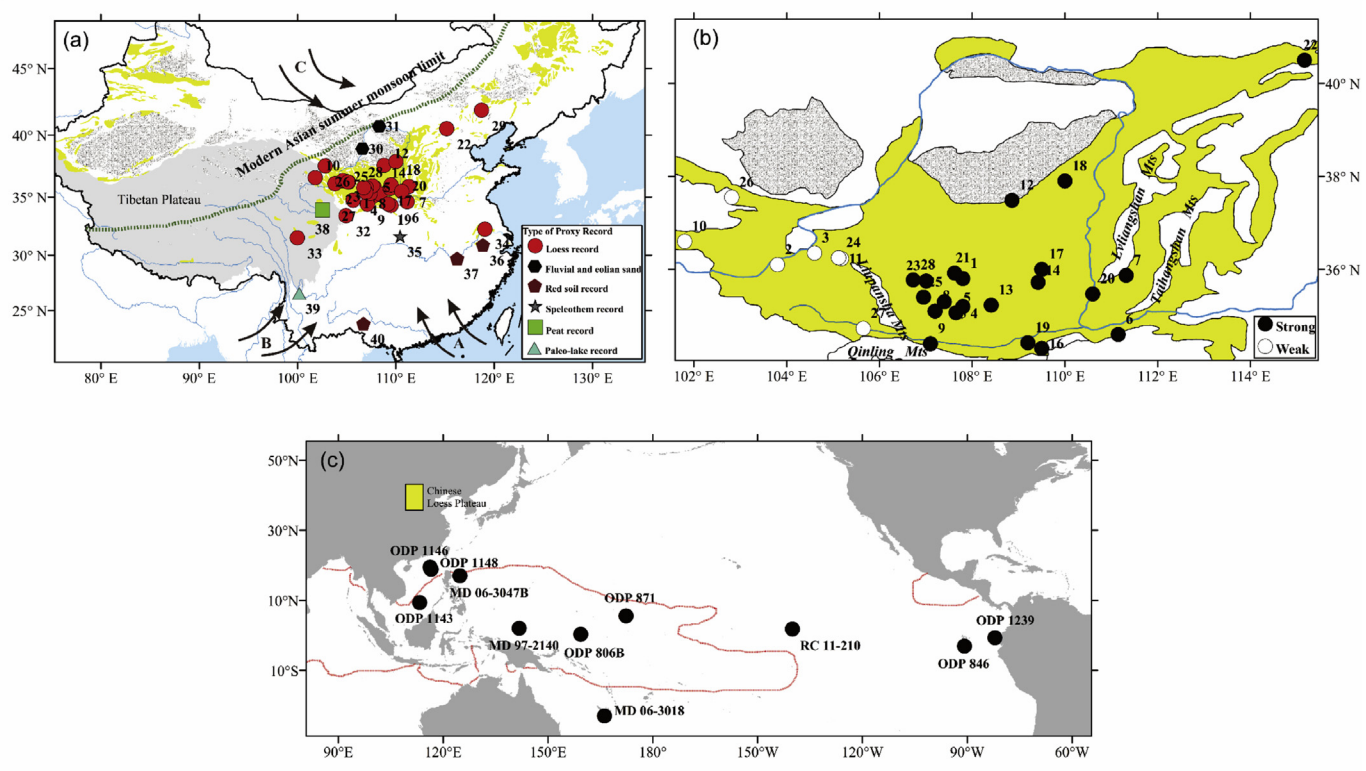

Fig. 2. Map of the study area and compilation of paleoclimate record sites. (a) Distribution and types of proxy records for MIS-13 in this study. A represents East Asian summer monsoon, B represents Indian summer monsoon and C represents East Asian winter monsoon. The modern Asian summer monsoon limit (thick dashed line) is modified from Chen et al. (2010). (b) Spatial distribution of soil development intensity for S5-1 paleosol in Chinese Loess Plateau. The bottom panel (c) shows the locations of SST record sites (black circles) in Tropical Pacific. The yellow rectangle in panel (c) indicates the location of the Chinese Loess Plateau shown in panel (a) and (b). The red dash line is the modern boundary of the Western Pacific Warm Pool, which is defined by annual sea surface temperature (SST) as 28 °C. Sites number according to Table 1. (For interpretation of the references to color in this figure legend, the reader is referred to the Web version of this article.)

pedogenic intensity of paleosol in the CLP.

This study is based primarily on compilation of paleoclimatic records from published literature. Records must meet several criteria in order to be included in our compilation. First, the sites must obviously be located in the CLP. Second, the records have to be derived from paleosol development or other proxies inferred from loess-paleosol sequences related to the intensity of pedogenesis in the CLP. Among various indicators applied to the CLP loess-paleosol sequences, MS has been widely used to indicate the intensity of loess and paleosol development because the product of newly-generated, fine-grained and strongly-magnetic particles that are related to pedogenic activity have been widely regarded as the major factor enhancing MS in the soil units (e.g., Zhou et al., 1990; Maher and Thompson, 1991). We do not exclude other proxies that could reflect pedogenesis intensity and climate condition, for example, environmental magnetism and geochemistry proxies. Third, in all proxies, the S5-1 and S4 paleosol units or the time stages of MIS-13 and MIS-11 must be able to be distinguished.

In addition, some records from other regions of monsoonal China are also selected to investigate the spatial variation of the EASM intensity. Together with the records from the CLP, our compilation includes in total 40 sites, including 28 loess-paleosol sections from the CLP and 7 paleo-soil sections, 4 drill cores and 1 speleothem record from other regions of monsoonal China (Fig. 2a and Table 1). Among the 28 CLP sections, 25 sections having MS records are used for the study of the spatial distribution of MS during MIS-13 and MIS-11, the other 3 sections containing other proxies being used for comparison (Table 1). The MS contour maps

Table 1
Proxy soil pedogenesis intensity or paleo-moisture records used in this study, Site number is given separately for Chinese Loess Plateau (1–28) and other regions of monsoonal China (29–40), as in Fig. 2a.

Number	Site	Record	Lat. (°N)	Long. (°E)	Proxies	Dating method	Reference
1	Xifeng	Loess	35.8	107.8	MS, Fed/Fet, grain size	MS age model	Guo et al. (2009)
2	Jiuzhoutai	Loess	36.1	103.8	MS, chromaticity, OM, $CaCO_3$, soil morphology description	Grain size age model	Chen and Zhang, 1993; Chen et al. (2014)
3	Jingyuan	Loess	36.35	104.6	MS, grain size, OM, $CaCO_3$, TOC	Orbital tuning	Sun et al. (2006a); Shi et al. (2013)
4	Changwu	Loess	35.2	107.8	MS, Fed/Fet, grain size	MS age model	Guo et al. (2009)
5	Lingtai	Loess	35.067	107.65	MS, grain size	Paleomagnetism	Sun et al. (2006b)
6	Caocun	Loess	34.6	111.15	Magnetic parameters	Paleomagnetism	Wang et al. (2006)
7	Miaoxia	Loess	35.87	111.32	Soil morphology description, MS	Paleomagnetism	Wang et al. (2000a)
8	Chaona	Loess	35.1	107.2	MS, grain size	Paleomagnetism	Han et al. (2012)
9	Baoji	Loess	34.4	107.1	Magnetic parameters, Rb/Sr, hematite (%), goethite (%)		Liu and Ding (1998); Guo et al. (2013)
10	Xining	Loess	36.6	101.8	MS, soil morphology description	Paleomagnetism	Li and Nie, 1999; Lu et al. (2012)
11	Duanxian	Loess	36.23	105.18	MS, soil morphology description, grain size	Paleomagnetism	Yang et al. (2002); Yang et al. (2006)
12	Jingbian	Loess	37.6	108.8	MS, grain size	Orbital tuning	Ding et al. (2005)
13	Xunyi	Loess	35.23	108.41	MS	Paleomagnetism	Xue et al. (2003)
14	Luochuan	Loess	35.72	109.42	MS, χ_{fd}, grain size	Grain-size age model	Hao et al. (2012)
15	Jingchuan	Loess	35.3	107.4	MS, grain size	Paleomagnetism	Ding et al. (2001b)
16	Weinan	Loess	34.3	109.5	MS	Paleomagnetism	Liu and Ding (1998)
17	Jiaodao	Loess	36	109.5	MS, χ_{fd}, Fed/Fet		Vidic et al. (2000)
18	Shimao	Loess	37.9	110	MS, grain size, soil morphology description	Paleomagnetism, TL	Sun et al. (1999)
19	Duanjiapo	Loess	34.42	109.2	MS, $\delta^{13}C$, OM, TOC		Lin and Liu, 1992
20	Laozhuang	Loess	35.47	110.6	MS, grain size	Paleomagnetism	Zhu et al. (2008)
21	Yimaguan	Loess	35.92	107.62	MS, χ_{fd}, grain size	Grain-size age model	Hao et al. (2012)
22	Fanshan	Loess	40.5	115.167	MS, grain size, soil morphology description	Paleomagnetism	Xiong et al. (2001)
23	Zhaojiachuan	Loess	35.75	107.008	MS, grain size	Paleomagnetism	Sun et al. (2006b)
24	Huining	Loess	36.25	105.12	MS	Paleomagnetism	Peng et al. (2015)
25	Baishui	Loess	35.4	106.95	MS		Xiong et al. (2002)
26	Shagou	Loess	37.55	102.817	Redness, grain size	TL, ^{14}C	Wu et al. (2001)
27	Zhongtan	Loess	34.727	105.651	Soil morphology description, grain size		Liu et al. (2007)
28	Pengyang	Loess	35.772	106.728	Chromaticity, LOI, $CaCO_3$	Paleomagnetism	Sui (2006)
29	Niuyangzigou	Loess	41.917	118.717	MS, grain size	OSL, Paleomagnetism	Lin et al. (2017)
30	Yinchuan Basin	Sediment	38.924	106.601	Pollen	Paleomagnetism	Li et al. (2017a)
31	Hobq Desert	Fluvial and eolian sand	40.674	108.308	Sediment redness, grain size	ESR, Paleomagnetism	Li et al. (2017b)
32	Wudu	Loess	33.42	104.92	MS, grain size, soil morphology description	^{14}C, TL/OSL, Paleomagnetism	Fang et al., 1999
33	Ganzi	Loess	31.52	99.98	CIA, Na/K, Fe^{2+}/Fe^{3+}, MS	OSL, Paleomagnetism	Qiao et al. (2010)
34	Dagang	Xiashu loess	32.26	119.055	CIA, $(CaO^* + Na_2O + MgO)/TiO_2$, Hm/Gt%, magnetic parameters	OSL, Paleomagnetism	Zhang et al. (2009)
35	Sanbao Cave	Stalagmite	31.667	110.433	Speleothem $\delta^{18}O$	^{230}Th	Cheng et al. (2016)
36	Xuancheng	Red soil	30.9	118.85	Soil micromorphology, XRD, chemical composition analysis, SEM	OSL, ESR	Yin and Guo (2006); Hong et al. (2010)
37	Jiujiang	Red soil	29.71	116.23	XRD, major element analysis, trace element analysis	OSL, ESR	Yin et al. (2017)
38	Zoige Basin	Lacustrine and fluvial	33.9	102.533	MS, carbonate content, pollen	^{14}C, TL/OSL, Paleomagnetism	Chen et al. (1999)
39	Heqing Basin	Paleo-lake	26.56	100.17	TOC, Rb/Sr, pollen	Paleomagnetism	An et al. (2011)
40	Bose	Red soil	23.77	106.7	Soil micromorphology, XRD, chemical composition analysis	$^{40}Ar/^{39}Ar$	Yin and Guo (2006)

are constructed using the Kriging interpolation in the ArcGIS 10.2 software package.

3. Results

3.1. The contrast of the S5-1 paleosol development between east-central and western CLP

In east-central CLP, many studies have found that S5-1 is the most prominent development paleosol by using mineral magnetism, geochemistry and soil mineralogy proxies and it can be easily recognized by its thickness and dark red color (e.g. Liu, 1985; An et al., 1987) (Fig. 2b and Table 1). By contrast, in the western CLP, different soil properties show that the S4 paleosol is obviously stronger developed than S5-1, although the loess deposits in the western CLP have been paid less attention and there are only a few sections. For example, in the Jiuzhoutai section (Fig. 2b and Table 1), the thickness of the S4 paleosol is 3.5 m, while the S5-1 is only 1.20 m (Chen and Zhang, 1993). Moreover, the S4 is reddish brown to red brown exhibiting fine prismatic to fine subangular blocky structure, carbonate hyphaetubular and calcareous nodules scattered, while the S5-1 paleosol is reddish brown, with prominent prism and prismatic structure, the carbonate nodule particles scattered, and containing many white and black spots (Chen and Zhang, 1993). Laboratory measurement also show that the magnetic susceptibility of S5-1 is higher than that of its overlying loess layer, but is obviously lower than that of upper paleosol layers (Sun et al., 2006a) (Fig. 1b). The redness of S5-1 paleosol is obviously lower than S4 (Shi et al., 2013; Wu et al., 2001). The $CaCO_3$ content of S5-1 is higher than overlying loess layers, the peak value is located in the mid-upper part of S5-1 paleosol unit, and $CaCO_3$ is mostly concentrated on the surface, suggesting that the effective precipitation is low during soil development (Chen and Zhang, 1993; Shi et al., 2013). The content of organic matters in S5-1 is lower than other paleosols from S4 to S1, suggesting a low biological productivity (Chen and Zhang, 1993; Shi et al., 2013). Therefore, contrary to the central CLP, the S5-1 paleosol is weakly developed in the western CLP while the S4 paleosol (developed during MIS-11) is the most developed in the Quaternary loess-paleosol sequences (Chen and Zhang, 1993; Sun et al., 2006a; Shi et al., 2013) (Fig. 2b and Table 1). In line with the evidence from loess records, a climate-soil combined model, which was used to simulate the soil formation of MIS-13 on the CLP, showed that regional diversity existed in the relative intensity of the S5-1 soil formation and that weak soil development was simulated in the western CLP (Finke et al., 2017).

3.2. Spatial change of the monsoon climate indicated by magnetic susceptibility during MIS-13 and MIS-11

The MS records from continuous loess-paleosol sequences have been widely used as an indicator of changes in monsoon precipitation (Liu, 1985; An et al., 1990; Chen et al., 1991; Hao and Guo, 2005), and thus the temporal and spatial changes of MS should primarily reflect the effects of the summer monsoon. Therefore, here we use the maximum MS value of the S5-1 and S4 paleosols to compile the MS contour maps and to reflect the spatial variation of the EASM intensity.

Based on the MS records of 25 sections, the spatial change of MS across the CLP is examined. The MS contour maps of MIS-13 and MIS-11 share two common features (Fig. 3). First, the isolines of MS exhibit a northeast-southwest zonal spatial distribution pattern and are convex toward the northwest. Second, MS increases consistently from northwest to southeast and is highly consistent

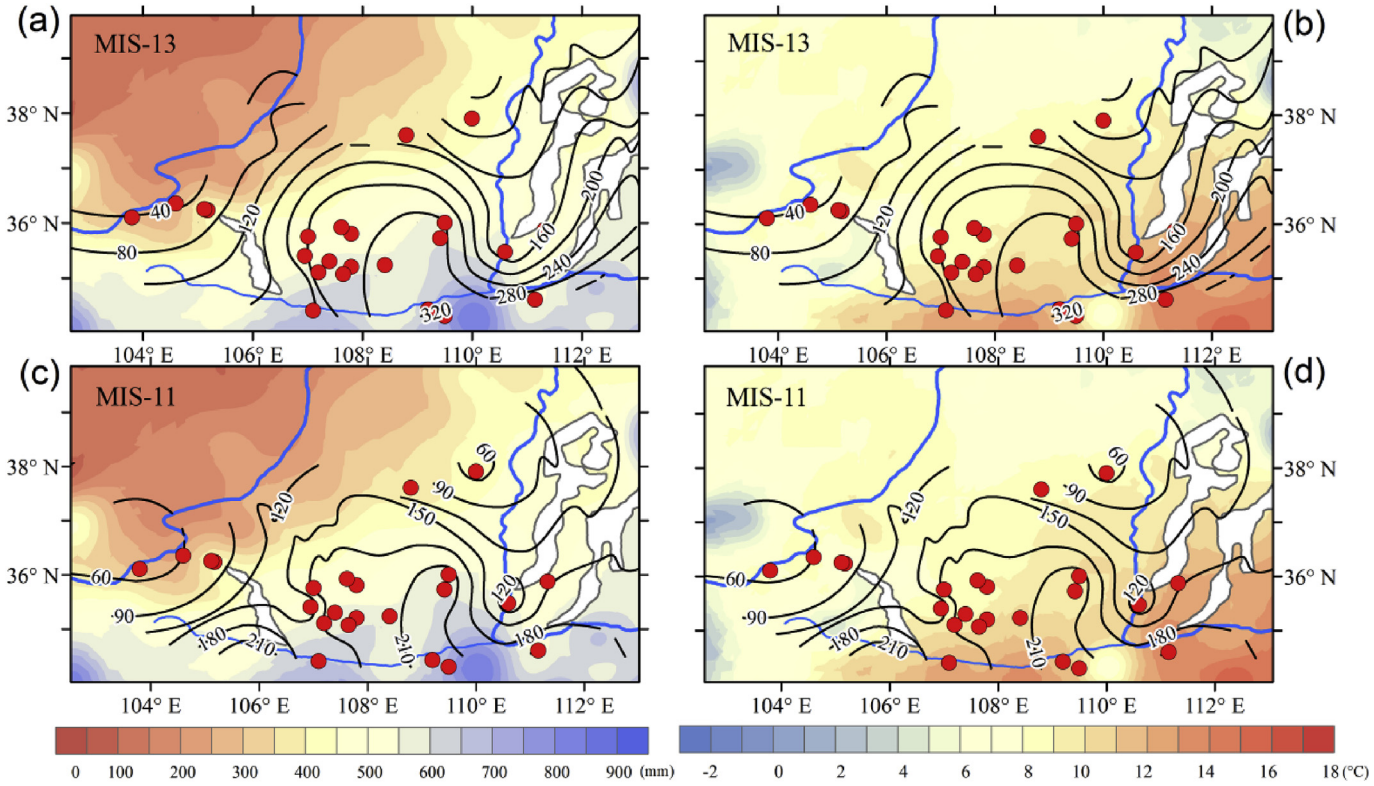

Fig. 3. Magnetic susceptibility (10^{-8} m^3 kg^{-1}) contour maps for the MIS-13 (a and b) and MIS-11 (c and d), together with modern mean annual precipitation (a and c) and temperature (b and d) over 51 y (1951–2001). The contour maps were constructed using magnetic susceptibility data from 25 loess sections.

with the distribution of present-day annual precipitation and temperature in the CLP. These similarities demonstrate that the MS records of both MIS-13 and MIS-11 are controlled by the same summer monsoon regime. However, two differences between the two time intervals are noteworthy (Fig. 3). First, the spatial variation of the MS values is greater during MIS-13 (from $40 \times 10^{-8}\ m^3\ kg^{-1}$ in the northwest to $>280 \times 10^{-8}\ m^3 \cdot kg^{-1}$in the southeast) than during MIS-11 (from $60 \times 10^{-8}\ m^3\ kg^{-1}$ to $>210 \times 10^{-8}\ m^3\ kg^{-1}$). Second, the MS values are significantly higher during MIS-13 than during MIS-11 in the east-central CLP, by ~$60 \times 10^{-8}\ m^3\ kg^{-1}$ to $80 \times 10^{-8}\ m^3\ kg^{-1}$ in the southeast, while in the western CLP, the MS values are lower during MIS-13 than during MIS-11, by $20 \times 10^{-8}\ m^3\ kg^{-1}$ to $40 \times 10^{-8}\ m^3\ kg^{-1}$ in northwest. These differences indicate a different pattern of the rain belt. In the east-central CLP, the $200–240 \times 10^{-8}\ m^3\ kg^{-1}$ isolines of MS are located more northwestward during MIS-13 than during MIS-11, indicating a stronger impact of the rain belt during MIS-13. However, in the western CLP, the $60–100 \times 10^{-8}\ m^3\ kg^{-1}$ isolines of MIS-13 have a similar location to MIS-11 or lower than MIS-11, indicating that the monsoon rain belt doesn't penetrate into the western CLP during MIS-13. In other words, different from the central CLP, the EASM has a weaker influence during MIS-13 than MIS-11 in the western CLP.

3.3. Spatial variation of the monsoon climate in other regions of monsoonal China during MIS-13

To better understand the variation of the EASM during MIS-13 in a larger space than the CLP, records from other regions of monsoonal China are used to compare with the CLP records. As shown in Fig. 4, in northern China, the loess records east of the modern 400 mm annual average isohyet, which is considered as the boundary semi-humid and semi-arid regions and as roughly the northern boundary of the average influence of the EASM (Chen et al., 1991), indicate extremely wet condition, suggesting a strong EASM precipitation during MIS-13. However, to the west of the modern 400 mm annual average isohyet, all the records indicate dry condition during MIS-13. In southern China, most of the records indicate a relatively humid environment during MIS-13 (Fig. 4). Specifically, along the lower reach of the Yangtze River around Nanjing and Zhenjiang, the eolian deposits named the Xiashu Loess are widely distributed (Liu, 1985; Li, 2006). Study of the iron oxide mineralogy of the Xiashu loess shows that the paleosols S5 and S4, corresponding to MIS-13 and 11, respectively, are the most developed, indicating strong summer monsoon (Zhang et al., 2007a, 2009). The Xiashu loess is gradually replaced by the so-called vermiculated red soil to the south (red clay with well-developed net-like veins) that occurs widely along the middle-lower reaches of the Yangtze River. In Xuancheng and Jiujiang, the vermiculated red soil was considered to have formed during Middle Pleistocene. The net-like veins are suggested to have formed in the same time of the S4 and S5 paleosols in the CLP, and indicate an extremely warm and humid climate associated with an unusually strong EASM based on soil micromorphological, mineralogical and chemical analyses (Yin and Guo, 2006; Hong et al., 2010, 2013; Hu et al., 2010; Yin et al., 2017). The loess records at Ganzi and Wudu from southwestern China also show that the S5-1 paleosol is the most developed (Qiao et al., 2010; Fang et al., 1999). The paleo-lake record in Heqing basin shows the Indian summer monsoon (ISM) is also so strong in this stage and it begins to be weaken during the interglacials after the MIS-11 by reconstruction of ISM index (An et al., 2011), indicating that loess development in the western CLP may be impossible to be affected by ISM. The stalagmite $\delta^{18}O$ record, which is usually used to reflect the EASM intensity, shows that MIS-13 is not extremely strong but as strong as the more recent intergalcials (Cheng et al., 2016).

4. Discussion

In summary, there are two paradoxes about the EASM for MIS-13: one is the strong EASM occurring in a relatively cool interglacial globally (Yin and Guo, 2008), and the other one is the

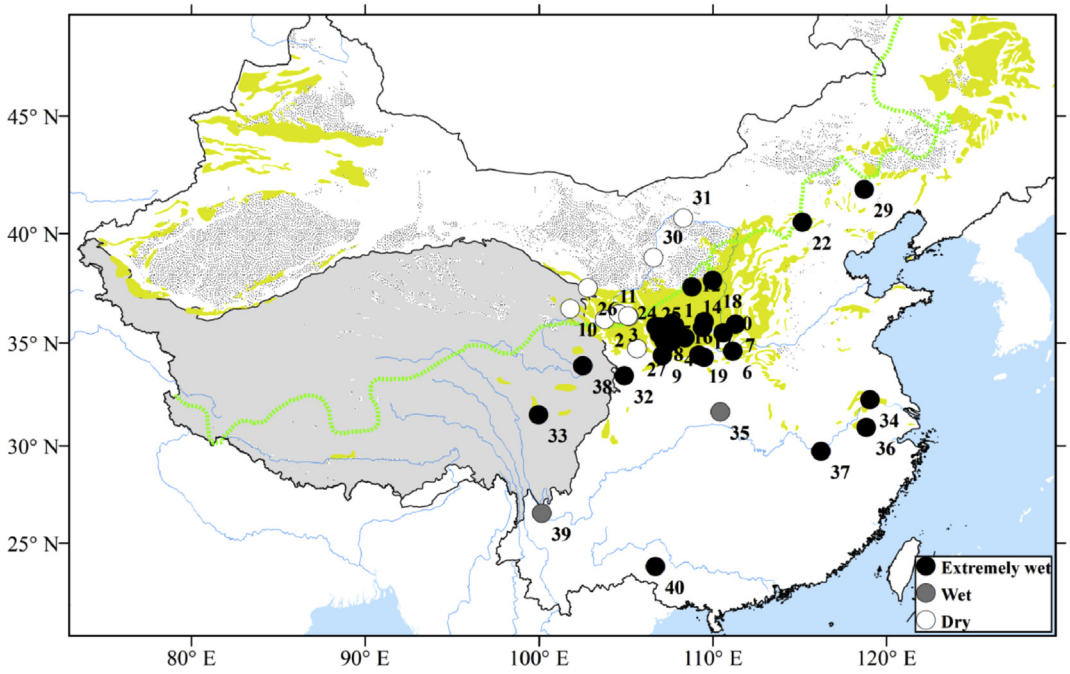

Fig. 4. Map showing the humidity condition indicated by paleoclimate records (numbered according to Table 1) during MIS-13. Humidity was classified into extremely wet, wet and dry. The thick dash line is the modern 400 mm annual average isohyet, representing roughly the northern boundary of the average condition of the East Asian summer monsoon.

inconsistency of the EASM intensity between the regions east and west of the summer monsoon boundary (the modern 400 mm annual average isohyet). They can be attributed to "the abnormal variability of the EASM".

What mechanisms are involved in producing the "the abnormal variability of the EASM"? Over the last several million years, the East Asian monsoon (EAM) variability was dominated by changes in solar insolation and Northern Hemisphere ice volume (e.g., An et al., 1990; Ding et al., 1995; Liu and Ding, 1998; An, 2000), as well as processes operating at much shorter and more abrupt timescales than the orbital scale (Porter and An, 1995; Guo et al., 1996; Chen et al., 1997; Ding et al., 1999; Wang et al., 2000b). Model results show that insolation alone does not make the MIS-13 EASM exceptionally strong (Yin and Berger, 2012). The presence of a Eurasian ice sheet could slightly increase the precipitation in eastern China (Yin et al., 2008, 2009), but whether there were additional ice sheets in the Northern Hemisphere (NH) during MIS-13 is still unclear (Guo et al., 2009). It has also been speculated that the Tibetan Plateau had experienced an uplift around the Mid-Brunhes epoch and it might have played an important role in the stepwise enhancement the EASM (Han et al., 2012; Zhang et al., 2016). According to climate model simulations, Himalayan uplift can indeed lead to an enhancement in both the summer and winter Asian monsoons (An et al., 2001). However, intensification of the East Asian winter monsoon is not recognized in our study or over the CLP (Sun et al., 2006a) (Fig. 1e). Fluctuations in the percentages of Picea and Abies records, which reflect changes in the vegetation and environment of high elevation areas, do not reveal uplift of the northeastern Tibetan Plateau at 0.5 Ma (Li et al., 2017a). In addition, the uplift of the Tibetan Plateau occurred mainly in the Miocene and earlier rather than in the Pleistocene (Coleman and Hodges, 1995; Sun et al., 2015), indicating that the uplift of the Tibet Plateau was probably not the main factor controlling EASM since 2.6 Ma.

The EASM precipitation in China is also influenced by changes in the El Niño-Southern Oscillation (ENSO) system (Wang et al., 2000c; Chang et al., 2000; Yang and Lau, 2004; Li et al., 2017c). The ENSO cycle, alternating between La Niña and El Niño events, dominates the East Asia precipitation on inter-annual timescales. During the La Niña phase, Walker circulation strengthens, and rainfall increases in northern China (including the CLP) due to a northward migration of a subtropical ridge in western North Pacific (Chang et al., 2000; Yang and Lau, 2004). Conversely, during the El Niño phase, Walker circulation is weaker and rainfall decreases in northern China. It has been proposed that the ENSO-like events may cause anomalous EASM variability in much longer timescales (e.g., orbital and tectonic timescales) (Burls and Fedorov, 2014; Karami et al., 2015; Yu et al., 2016; Zhang et al., 2007b; Meng et al., 2018). Here we will discuss the temperature condition of the tropical Pacific Ocean during the interglacials since MIS-13 by comprehensive analysis of published sea surface temperature (SST) results (Table S1).

4.1. La Niña-like or El Niño-like during MIS-13?

Based on model simulations, Karami et al. (2015) suggested that, as compared to Pre-Industrial time, the mean climate state in the tropical Pacific during MIS-13 was La Niña-like. They found that this kind of SST condition especially cooler SST in central tropical Pacific during MIS-13 is favorable for the intensification of the EASM through its promotion of an upper-level teleconnection between the tropical Pacific Ocean and the EASM and also the strengthening of the northern Pacific subtropical high. This mechanism could possibly explain the strong EASM during MIS-13 as observed from the loess records in eastern CLP. However, this needs to be studied in the framework of the comparison of MIS-13 with other interglacials.

In modern tropical Pacific Ocean, the Western Pacific Warm Pool (WPWP) is characterized by annual SST above 28 °C and is the world's largest center of tropical convection. The spatial and temporal evolution of the WPWP is closely linked to large-scale climatic features, such as the ENSO from seasonal to geological time scales (Barlow et al., 2002; de Garidel-Thoron et al., 2005). Based on published SST results, we find that the maximum value of SST from MD 97-2140 core, which is located in the west of modern WPWP center, is higher during the interglacials MIS-13 than during interglacials MIS-11, MIS-9 and MIS-7, whereas the maximum value of SST from other cores, which are mainly distributed around the WPWP, are on the contrary (Figs. 1c and 5). Therefore, we may infer the WPWP area is smaller and high center is west during MIS-13 compared with other interglacials. However, in the eastern tropical Pacific, the reconstructed maximum value of SST is not significantly different between MIS-13, MIS-11, MIS-9 and MIS-7, indicating similar sea surface condition in this region during these

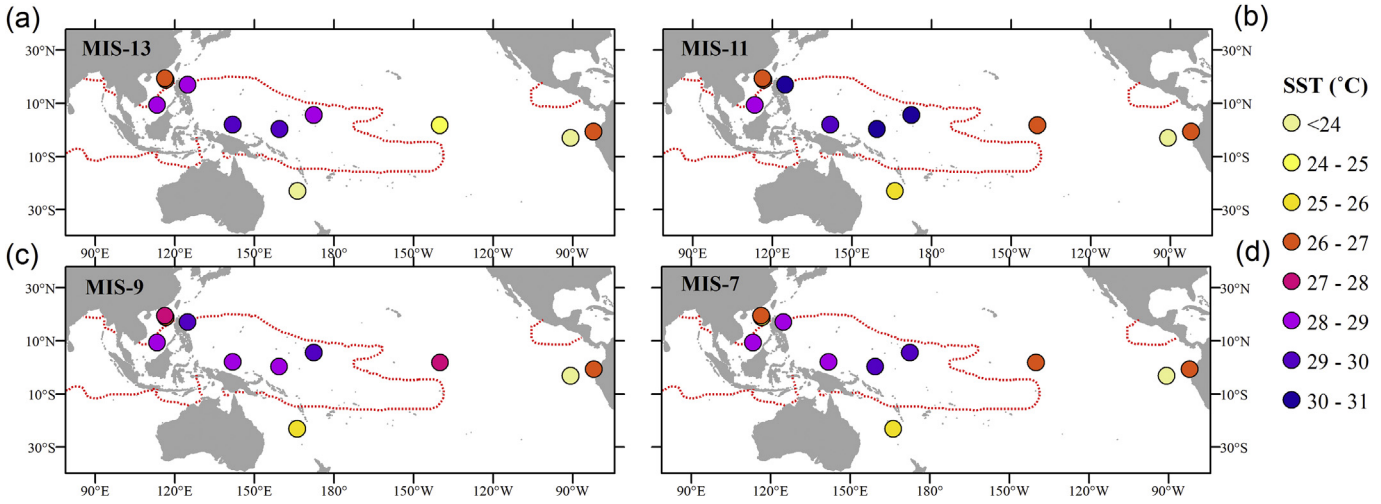

Fig. 5. Maps show spatial changes of the maximum value of sea surface temperature (SST) for interglacials MIS-13 (a), MIS-11 (b), MIS-9 (c) and MIS-7 (d) from different ocean drilling records (Table 1S) in the Tropical Pacific, the red lines are 28 °C isolines. (For interpretation of the references to color in this figure legend, the reader is referred to the Web version of this article.)

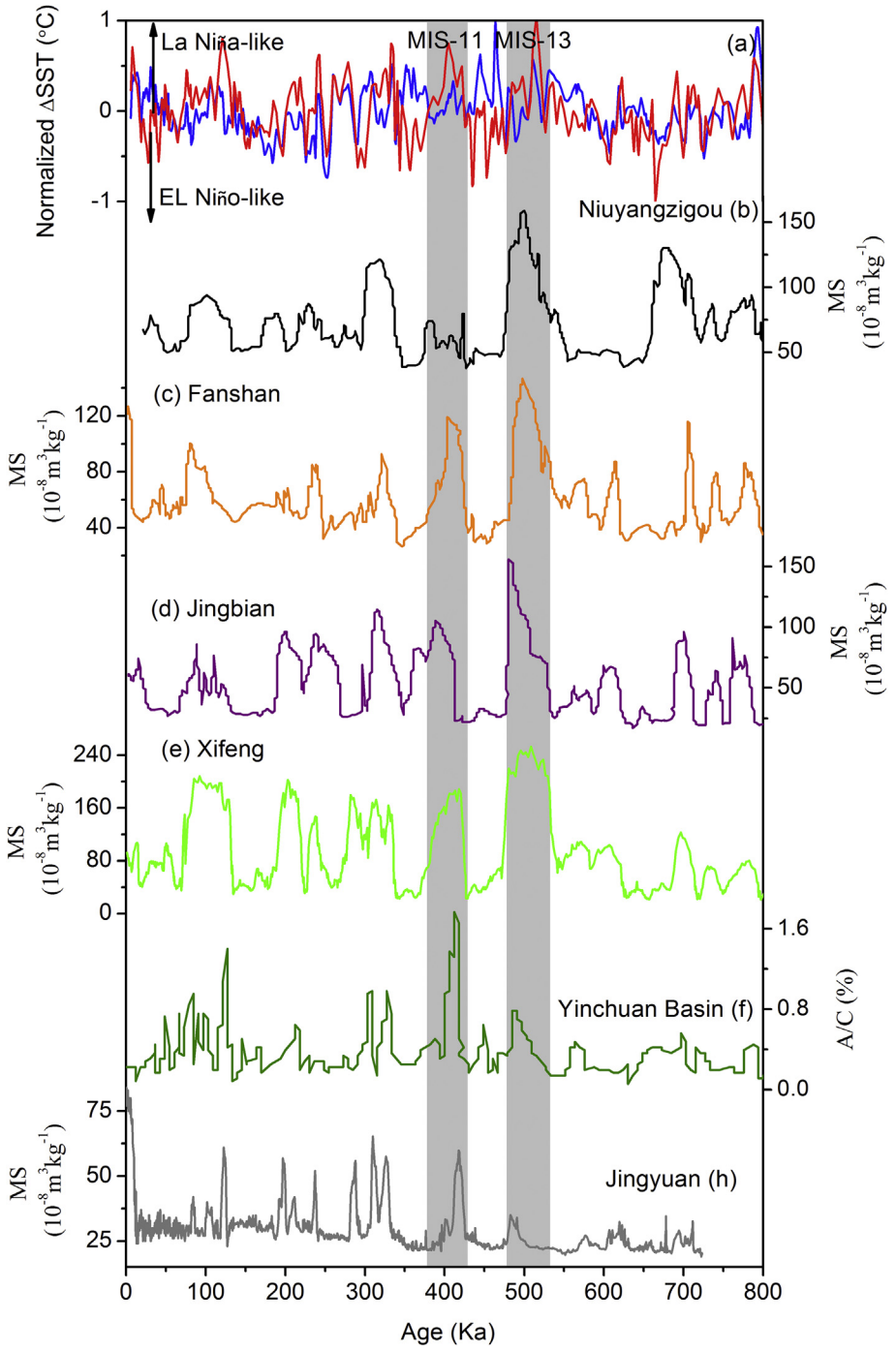

Fig. 6. The comparison of zonal SST gradients (ΔSST) between MD97-2140 (de Garidel-Thoron et al., 2005) and RC11-210 (Pisias and Rea, 1988) (red curve), MD97-2140 and ODP846 (blue curve) (a) with magnetic susceptibility records in Niuyangzigou section (Lin et al., 2017) (b), Fanshan section (Xiong et al., 2001) (c), Jingbian section (Ding et al., 2005) (d), Xifeng section (Guo et al., 2009) (e), Jingyuan section (Sun et al., 2006a) (h) and pollen records in Yinchuan Basin (Li et al., 2017a) (f). Gray frame denote the proxies for which MIS-13 and MIS-11 are contrasted in the paper. (For interpretation of the references to color in this figure legend, the reader is referred to the Web version of this article.)

interglacials (Figs. 1c and 5). By contrast, the variability of maximum SST from the RC-11240 core, located in the central tropical Pacific of Niño 3.4 region, is more prominent than that of ODP846 site, located in Niño 1 or 2 regions (Figs. 1c and 5), suggesting that the Pacific cold tongue has shifted westward during MIS-13. All these indicate that the mean climate of MIS-13 is likely La Niña-like or to be precise it is central La-Niña (La Niña Modoki) type. The relatively smaller and more westwards located center of the WPWP during MIS-13 could weaken the WPSH with its west ridge retreating more northeastward to strengthen the EASM (Huang and Sun, 1992; Lu and Dong, 2001). Meanwhile, the relatively cool SST in the central tropical Pacific Ocean during MIS-13 could also provide more rainfall over EASM through maintaining the teleconnection between the tropical Pacific and EASM, as suggested by Karami et al. (2015).

In modern ocean studies, different types of ENSO events generally occur in the central and eastern tropical Pacific. Therefore, here we use the zonal sea SST gradients (ΔSST) between the

Western Equatorial Pacific Warm Pool, Central Equatorial Pacific and the East Equatorial Pacific cold tongue as the Central ENSO index and Eastern ENSO index. This gradient can be calculated by using reconstructed paleo-temperature based on planktonic foraminiferal Mg/Ca ratios and alkenone data from the MD 97-2140 (Mg/Ca) in the western Pacific, the RC11-210 (radiolarian fauna analysis) in the central Pacific and the ODP 846 (alkenone) in the eastern Pacific (Fig. 1c and Table S1) (de Garidel-Thoron et al., 2005; Pisias and Rea, 1988; Liu and Herbert, 2004). Although the temporal resolution of these records is not very high, the normalized SST gradients of Central ENSO reach the maximum during MIS-13, gradually decrease during the interglacials after MIS-13, and then begin to increase during MIS-5 (Fig. 6a). However, the normalized SST gradients of Eastern ENSO index show ΔSST is lower than Central ENSO index during MIS-13 and is not higher than other interglaicls. Although a more La Niña-like condition during MIS-13 relative to the present has been suggested by some model simulations under the MIS-13 insolation forcing (Muri et al., 2013; Karami et al., 2015), there was no study having shown an exceptionally strong La Niña-like condition during MIS-13 as compared to other interglacials including MIS-11, MIS-9 and MIS-7. What has caused the MIS-13 exceptional La Nina-like condition remains to be investigated, but in the meantime it could offer an explanation for the EASM abnormality during MIS-13 as explained in the next section.

4.2. Influence of exceptional La Niña-like climatic state on the abnormality of the EASM during MIS-13

The maximum of zonal ΔSST indicates a stronger La Nina-like condition during MIS-13 than other interglacials, corresponding to a strong EASM and extremely humid environment as shown by the loess records in the east of the modern annul average 400 mm isohyet in northern China (Fig. 6a, b, c, d and e). By contrast, during MIS-11, weaker La Nina-like condition corresponds to weaker EASM but wetter condition to the west of the modern annual average 400 mm isohyet (Fig. 6a, f and h). This precipitation spatial distribution difference between MIS-13 and MIS-11 is similar to the difference between strong La Niña years and weak ones in modern observation (Fig. 7).

Numerous studies have shown that ENSO could affect the EASM rain belt through its influence on the Western Pacific Subtropical High (WPSH) (Huang and Wu, 1989; Wang et al., 2000c; Tao and Wei, 2006; Qian et al., 2007; Karami et al., 2015). It has been found that during the La Niña phase, Walker circulation strengthens and the WPSH becomes weak with its west ridge retreating more northeastward (Lu and Dong, 2001; Qian et al., 2007; Ding et al., 2008; Tan and Nan, 2010). This leads to a northeastward shift of the EASM rain belt and consequently more precipitation most regions of monsoonal China especially in the mid-east region of northern China in mid-summer. In contrast, during the El Niño phase, Walker circulation is weaker and the WPSH becomes stronger with its west ridge extending more westward, leading to less rainfall in the mid-east region of northern China (Lu and Dong, 2001; Qian et al., 2007; Ding et al., 2008; Tan and Nan, 2010). The spatial difference in the EASM precipitation between MIS-13 and MIS-11 can therefore be explained by a stronger La-Niña-like condition during MIS-13. Under stronger La-Niña condition, the WPSH could become weaker and retreat more northeastward, leading to more precipitation in the mid-east region of northern China (including the east-central CLP) and preventing the penetration of the EASM rain belt into the northwestern inland.

5. Conclusions

Compilation of proxy records from the CLP show that the relative intensity of the S5-1 and S4 paleosols is different between the east-central and the western CLP. In the western CLP, the S5-1 paleosol is weakly developed whereas the S4 paleosol is the most developed. However, it is the contrary in the central CLP.

Magnetic susceptibility isolines in the CLP and other records from the monsoonal China indicate that the northern front of the EASM during MIS-13 did not penetrate into the western CLP, but is located more northerly in the eastern part of northern China.

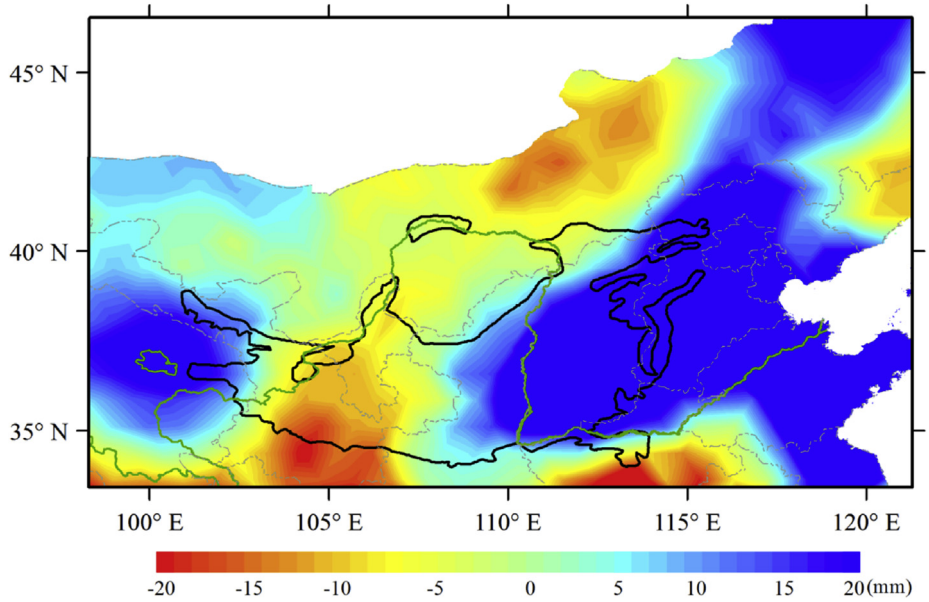

Fig. 7. Modern summer average precipitation spatial distribution difference (mm/day) between all the strong La Niña years and weak La Niña years from 1961 to 2014. The strong La Niña years and weak La Niña years are defined by Mei index and are ranked by the value of winter SST (https://www.esrl.noaa.gov/psd/enso/climaterisks/years/top24enso.html); the precipitation data is obtained from 824 observational stations in China for the period 1961 to 2014, archived and updated by the China Meteorological Administration (http://data.cma.cn/data/cdcdetail/dataCode/SURF CLI CHN MUL DAY V3.0.html).

The SST reconstructions over the tropical Pacific indicate a strong La Niña-like condition during MIS-13, which could explain the abnormality of the EASM during MIS-13. A strong La Niña-like condition could cause a weaker but more northeastward located WPSH leading to more precipitation in the mid-east region of northern China (including the east-central CLP) in the mid-summer and preventing the penetration of the EASM rain belt into the northwestern inland.

Our results highlights the necessity of using high-resolution or regional climate models in understanding the regional EASM variability during MIS-13 and the importance of understanding the tropical oceanic dynamics during this interglacial and its link with global climate.

Acknowledgements

This work is supported by National Key Research and Development Program of China (Grant 2018YFA0606401), the Open Foundation of MOE Key Laboratory of Western China's Environmental System, Lanzhou University and the Fundamental Research Funds for the Central Universities (lzujbky-2017-kl01), China Scholarship Council (CSC) under the file number 201706180099 and the Fonds de la Recherche Scientifique-FNRS under grant MIS F.4529.18, Belgium. Q.Z. Yin acknowledges the support from the Fonds de la Recherche Scientifique-FNRS.

Appendix A. Supplementary data

Supplementary data to this article can be found online at https://doi.org/10.1016/j.quascirev.2019.106048.

References

An, Z.S., Liu, T.S., Zhu, Y.Z., Sun, F., 1987. The paleosol complex S5 in the China Loess Plateau – a record of climatic optimum during the last 1.2 Ma. Geojournal 15, 141–143.
An, Z.S., Liu, T.S., Lu, Y.C., Porter, S.C., Kukla, G., Wu, X.H., Hua, Y.M., 1990. The long-term paleomonsoon variation recorded by the loess-paleosol sequence in central China. Quat. Int. 7, 91–95.
An, Z.S., 2000. The history and variability of the East Asian paleomonsoon climate. Quat. Sci. Rev. 19, 171–187.
An, Z.S., Porter, S.C., Kutzbach, J.E., Wu, X.H., Wang, S.M., Liu, X.D., Zhou, W.J., 2000. Asychronous Holocene optimum of the east Asian monsoon. Quat. Sci. Rev. 19, 743–762.
An, Z.S., Kutzbach, J.E., Prell, W.L., Porter, S.C., 2001. Evolution of Asian monsoons and phased uplift of the Himalaya-Tibetan plateau since late Miocene times. Nature 411, 62–66.
An, Z.S., Clemens, S.C., Shen, J., Qiang, X.K., Jin, Z.D., Sun, Y.B., Prell, W.L., Luo, J.J., Wang, S.M., Xu, H., Cai, Y.J., Zhou, W.J., Liu, X.D., Shi, Z.G., Yan, L.B., Xiao, X.Y., Chang, H., Wu, F., Ai, L., Lu, F.Y., 2011. Glacial-interglacial Indian summer monsoon dynamics. Science 333, 719–723.
Bassinot, F.C., Labeyrie, L.D., Vincent, E., Quidelleur, X., Shackleton, N.J., Lancelot, Y., 1994. The astronomical theory of climate and the age of the Brunhes-Matuyama magnetic reversal. Earth Planet. Sci. Lett. 126, 91–108.
Barlow, M., Cullen, H., Lyon, B., 2002. Drought in central and southwest Asia: La Niña, the warm pool, and Indian Ocean precipitation. J. Clim. 15, 697–700.
Berger, A., Loutre, M.F., 1991. Insolation values for the climate of the last 10 million years. Quat. Sci. Rev. 10, 297–317.
Bronger, A., Winter, R., Heinkele, T., 1998. Pleistocene climatic history of East and Central Asia based on paleopedological indicators in loess–paleosol sequences. Catena 34, 1–17.
Bronger, A., 2003. Correlation of loess–paleosol sequences in east and central Asia with SE Central Europe: towards a continental Quaternary pedostratigraphy and paleoclimatic history. Quat. Int. 106–107, 11–31.
Buggle, B., Hambach, U., Glaser, B., Gerasimenko, N., Marković, S., Glaser, I., Zöller, L., 2009. Stratigraphy, and spatial and temporal paleoclimatic trends in Southeastern/Eastern European loess–paleosol sequences. Quat. Int. 196, 86–106.
Burls, N.J., Fedorov, A.V., 2014. Simulating Pliocene warmth and a per-manent El Niño-like state: the role of cloud albedo. Paleoceanography 29, 893–910. https://doi.org/10.1002/2014PA002644.
Chang, C.P., Zhang, Y., Li, T., 2000. Interannual and interdecadal variations of the east Asian summer monsoon and tropical Pacific SSTs. Part II: meridional structure of the monsoon. J. Clim. 13, 4326–4340.
Chen, F.H., Zhang, W.X., 1993. Loess Stratigraphy and Quaternary Glaciation in Gansu-Qinghai Provinces. Science Press, Beijing, pp. 1–155 (in Chinese).
Chen, F.H., Bloemendal, J., Wang, J.M., Li, J.J., Oldfield, F., Ma, Y.Z., 1997. High-resolution multi-proxy climate records from Chinese loess: evidence for rapid climatic changes over the last 75 kyr. Palaeogeogr. Palaeoclimatol. Palaeoecol. 130, 323–335.
Chen, F.H., Bloemendal, J., Zhang, P.Z., Liu, G.X., 1999. An 800 ky proxy record of climate from lake sediments of the Zoige Basin, eastern Tibetan Plateau. Palaeogeogr. Palaeoclimatol. Palaeoecol. 151, 307–320.
Chen, F.H., Feng, Z.D., Zhang, J.W., 2000. Loess particle size data indicative of stable winter monsoons during the last interglacial in the western part of the Chinese Loess Plateau. Catena 39, 233–244.
Chen, F.H., Chen, J.H., Holmes, J., Boomer, I., Austin, P., Gates, J.B., Wang, N.L., Brooks, S.J., Zhang, J.W., 2010. Moisture changes over the last millennium in arid central Asia: a review, synthesis and comparison with monsoon region. Quat. Sci. Rev. 29, 1055–1068.
Chen, J.S., Liu, X.M., Kravchinsky, V.A., 2014. Response of the high–resolution Chinese loess grain size record to the 50°N integrated winter insolation during the last 500,000 years. Geophys. Res. Lett. 41, 6244–6251.
Chen, L.X., Zhu, Q.G., Luo, H.B., He, J.H., Dong, M., Feng, Z.Q., 1991. Monsoon over East Asia, 362 pp. Meteorol. Publ., Beijing (in Chinese).
Cheng, H., Edwards, R.L., Sinha, A., Spötl, C., Liang, Y., Chen, S.T., Kelly, M., Kathaya, G., Wang, X.F., Li, X.L., Kong, X.L., Wang, Y.J., Ning, Y.F., Zhang, H.W., 2016. The Asian monsoon over the past 640,000 years and ice age terminations. Nature 534, 640.
Coleman, M., Hodges, K., 1995. Evidence for Tibetan plateau uplift before 14 Myr ago from a new minimum age for east–west extension. Nature 374, 49–52.
Ding, Y.H., Wang, Z.Y., Sun, Y., 2008. Inter-decadal variation of the summer precipitation in East China and its association with decreasing Asian summer monsoon. Part I: observed evidences. Int. J. Climatol. 28, 1139–1161.
Ding, Y.H., Si, D., Liu, Y.J., Wang, Z.Y., Li, Y., Zhao, L., Song, Y.F., 2018. On the characteristics, driving forces and inter-decadal variability of the East Asian summer monsoon. J. Atmos. Sci. 42, 533–558. https://doi.org/10.3878/j.issn.1006-9895.1712.17261 (in Chinese).
Ding, Z.L., Liu, T.S., Rutter, N.W., Yu, Z.W., Guo, Z.T., Zhu, R.X., 1995. Ice-volume forcing of East Asian winter monsoon variations in the past 800,000 years. Quat. Res. 44, 149–159.
Ding, Z.L., Ren, J.Z., Yang, S.L., Liu, T.S., 1999. Climate instability during the penultimate glaciation: evidence from two high resolution loess records, China. J. Geophys. Res. 104, 20123–20132.
Ding, Z.L., Yang, S.L., Sun, J.M., Liu, T.S., 2001a. Iron geochemistry of loess and red clay deposits in the Chinese Loess Plateau and implications for long-term Asian monsoon evolution in the last 7.0 Ma. Earth Planet. Sci. Lett. 185, 99–109.
Ding, Z.L., Yang, S.L., Hou, S.S., Wang, X., Chen, Z., Liu, T.S., 2001b. Magnetostratigraphy and sedimentology of the Jingchuan red clay section and correlation of the Tertiary eolian red clay sediments of the Chinese Loess Plateau. J. Geophys. Res. 106, 6399–6407.
Ding, Z.L., Ranov, V., Yang, S.L., Finaev, A., Han, J.M., Wang, G.A., 2002. The loess record in southern Tajikistan and correlation with Chinese loess. Earth Planet. Sci. Lett. 200, 387–400.
de Garidel-Thoron, T., Rosenthal, Y., Bassinot, F., Beaufort, L., 2005. Stable sea surface temperatures in the western Pacific warm pool over the past 1.75 million years. Nature 433, 294.
Ding, Z.L., Derbyshire, E., Yang, S.L., Sun, J.M., Liu, T.S., 2005. Stepwise expansion of desert environment across northern China in the past 3.5 Ma and implications for monsoon evolution. Earth Planet. Sci. Lett. 237, 45–55.
Fang, X.M., Li, J.J., Van der Voo, R., 1999. Rock magnetic and grain size evidence for intensified Asian atmospheric circulation since 800,000 years BP related to Tibetan uplift. Earth Planet. Sci. Lett. 165, 129–144.
Finke, P., Yin, Q.Z., Bernardini, N.J., Yu, Y.Y., 2017. Climate-soil model reveals causes of differences between Marine Isotope Stage 5e and 13 paleosols. Geology. https://doi.org/10.1130/G39301.1.
Guo, X.L., Liu, X.M., Li, P.Y Lü B., Guo, H., Chen, Q., Liu, Z., Ma, M.M., 2013. The magnetic mechanism of paleosol S5 in the Baoji section of the southern Chinese Loess Plateau. Quat. Int. 306, 129–136.
Guo, Z., Liu, T., Guiot, J., Wu, N., Lü, H., Han, J., Liu, J., Gu, Z., 1996. High frequency pulses of East Asian monsoon climate in the last two glaciations: link with the north Atlantic. Clim. Dyn. 12, 701–709.
Guo, Z.T., Liu, T.S., Fedoroff, N., Wei, L.Y., Ding, Z.L., Wu, N.Q., Lu, H.Y., Jiang, W.Y., An, Z.S., 1998. Climate extremes in loess of China coupled with the strength of deep-water formation in the North Atlantic. Glob. Planet. Chang. 18, 113–128.
Guo, Z.T., Berger, A., Yin, Q.Z., Qin, L., 2009. Strong asymmetry of hemispheric climates during MIS-13 inferred from correlating China loess and Antarctica ice records. Clim. Past 5, 21–31.
Han, W.X., Fang, X.M., Berger, A., 2012. Tibet forcing of mid-Pleistocene synchronous enhancement of East Asian winter and summer monsoons revealed by Chinese loess record. Quat. Res. 78, 174–184.
Hao, Q.Z., Guo, Z.T., 2005. Spatial variations of magnetic susceptibility of Chinese loess for the last 600 kyr: implications for monsoon evolution. J. Geophys. Res. 110.
Hao, Q.Z., Wang, L., Oldfield, F., Peng, S.Z., Qin, L., Song, Y., Xu, B., Qiao, Y.S., Bloemendal, J., Guo, Z., 2012. Delayed build-up of Arctic ice sheets during 400,000-year minima in insolation variability. Nature 490, 393.
Hong, H., Gu, Y.S., Li, R.B., Zhang, K.X., Li, Z.H., 2010. Clay mineralogy and geochemistry and their palaeoclimatic interpretation of the Pleistocene deposits in the Xuancheng section, southern China. J. Quat. Sci. 25, 662–674.
Hong, H., Gu, Y., Yin, K., Wang, C., Li, Z., 2013. Clay record of climate change since the

mid-Pleistocene in Jiujiang, south China. Boreas 42, 173–183.
Hu, Q., Jiang, D.B., Lang, X.M., Xu, B., 2016. Moisture sources of the Chinese loess plateau during 1979–2009. Palaeogeogr. Palaeoclimatol. Palaeoecol. https://doi.org/10.1016/j.palaeo.2016.12.030.
Hu, X.F., Wei, J., Du, Y., Xu, L.F., Wang, H.B., Zhang, G.L., Ye, W., Zhu, L.D., 2010. Regional distribution of the Quaternary Red Clay with aeolian dust characteristics in subtropical China and its paleoclimatic implications. Geoderma 159, 314–317.
Huang, R.H., Sun, F.Y., 1992. Impacts of the tropical western Pacific on the East Asian summer monsoon. J. Meteorol. Soci. Japan. Ser. II 70, 243–256.
Huang, R.H., Wu, Y.F., 1989. The influence of ENSO on the summer climate change in China and its mechanism. Adv. Atmos. Sci. 6, 21–32.
Jia, J.J., Lu, H., Wang, Y.J., Xia, D.S., 2018a. Variations in the iron mineralogy of a loess section in Tajikistan during the Mid–Pleistocene and Late Pleistocene: implications for the climatic evolution in Central Asia. Geochem. Geophys. Geosyst. 19, 1244–1258.
Jouzel, J., Masson-Delmotte, V., Cattani, O., Dreyfus, G., Falourd, S., Hoffman, G., Minster, B., Nouet, J., Barnola, J.M., Chappellaz, J., Fischer, H., Gallet, J.C., Johnsen, S., Leuenberger, M., Loulergue, L., Luethi, D., Oerter, H., Parrenin, F., Raisbeck, G., Raynaud, D., Schilt, A., Schwander, J., Selmo, E., Souchez, R., Spahni, R., Stauffer, B., Steffensen, J.P., Stenni, B., Stocker, T.F., Tison, J.L., Werner, M., Wolff, E.W., 2007. Orbital and millennial Antarctic climate variability over the past 800,000 years. Science 317, 793–796.
Karami, M.P., Herold, N., Berger, A., Yin, Q.Z., Muri, H., 2015. State of the tropical Pacific Ocean and its enhanced impact on precipitation over East Asia during marine isotopic stage 13. Clim. Dyn. 44, 807–825.
Kukla, G., An, Z.S., Melice, J.L., Gavin, J., Xiao, J.L., 1990. Magnetic susceptibility record of Chinese loess. Trans. R. Soc. Edinb. Earth Sci. 81, 263–288.
Li, B.F., Sun, D.H., Xu, W.H., Wang, F., Liang, B.Q., Ma, Z.W., Wang, X., Li, Z.J., Chen, F.H., 2017b. Paleomagnetic chronology and paleoenvironmental records from drill cores from the Hetao Basin and their implications for the formation of the Hobq Desert and the Yellow River. Quat. Sci. Rev. 156, 69–89.
Li, H.J., Gao, J.E., Zhang, H.C., Zhang, Y.X., Zhang, Y.Y., 2017c. Response of extreme precipitation to solar activity and El Nino events in typical regions of the Loess Plateau. Adv. Meteorol. https://doi.org/10.1155/2017/9823865.
Li, L.W., 2006. The Xiashu Loess and Paleo-Gravel Deposits Near Nanjing. Nanjing Normal University Press, Nanjing (in Chinese).
Li, X.L., Hao, Q.Z., Wei, M.J., Andreev, A.A., Wang, J.P., Tian, Y.Y., Li, X.L., Cai, M.T., Hu, J.M., Shi, W., 2017a. Phased uplift of the northeastern Tibetan Plateau inferred from a pollen record from Yinchuan Basin, northwestern China. Sci. Rep. https://doi.org/10.1038/s41598-017-16915-z.
Li, Z., Nie, S.R., 1999. Loess deposit at Xining and its provenance. J. Earth Sci. 24, 1–3 (in Chinese with English abstract).
Lin, B.H., Liu, R.M., 1992. The stable isotopic evidence of the monsoon variation on Chinese Loess Plateau since the last 800 ka years. Chin. Sci. Bull. 37, 178–182 (in Chinese).
Lin, Z., Lu, H.Y., Yi, S.W., Stevens, T., Xu, Z.W., Zhuo, H.X., Yu, K.F., Zhang, H.Z., 2017. Long-term Pleistocene aridification and possible linkage to high-latitude forcing: new evidence from grain size and magnetic susceptibility proxies from loess-paleosol record in northeastern China. Catena 154, 21–32.
Lisiecki, L.E., Raymo, M.E., 2005. A Pliocene-Pleistocene stack of 57 globally distributed benthic $\delta^{18}O$ records. Paleoceanography 20. https://doi.org/10.1029/2004PA001071.
Liu, T.S., 1985. Loess and the Environment. China Ocean Press, Beijing, pp. 1–467 (in Chinese).
Liu, T.S., Ding, Z.L., 1998. Chinese loess and the paleomonsoon. Annu. Rev. Earth Planet Sci. 26, 111–145.
Liu, X.F., Pan, B.T., Gao, H.S., Wang, Y., Wang, J.P., Zhang, H., Hu, C.S., 2007. Loess deposit feature and environmental change in Tianshui: Gansu province. J. Desert Res. 27, 374–378 (in Chinese with English abstract).
Liu, Z.H., Herbert, T.D., 2004. High-latitude influence on the eastern equatorial Pacific climate in the early Pleistocene epoch. Nature 427, 720.
Loulergue, L., Schilt, A., Spahni, R., Masson-Delmotte, V., Blunier, T., Lemieux, B., Barnola, J.M., Raynaud, D., Stocker, T.F., Chappellaz, J., 2008. Orbital and millennial-scale features of atmospheric CH_4 over the past 800,000 years. Nature 453, 383–386.
Lu, H., Jia, J., Wang, Y.J., Yin, Q.Z., Xia, D.S., 2018. The cause of extremely high magnetic susceptibility of the S5S1 paleosol in the central Chinese Loess Plateau. Quat. Int. 493, 252–257.
Lu, H.Y., Wang, X.Y., Wang, X.Y., Sun, X.F., Yi, S.W., Zhou, Y.L., Liu, Q.Y., Swinehart, J., Vandenberghe, J., 2012. Palaeoclimatic changes in northeastern Qinghai-Tibetan Plateau revealed by magnetostratigraphy and magnetic susceptibility analysis of thick loess deposits. Neth. J. Geosci. 91, 189–198.
Lu, R.Y., Dong, B.W., 2001. Westward extension of North Pacific subtropical high in summer. J. Meteorol. Soc. Jpn. Ser. II 79, 1229–1241.
Lüthi, D., Le, F.M., Bereiter, B., Blunier, T., Barnola, J.M., Siegenthaler, U., Raynaud, D., Jouzel, J., Fischer, H., Kawamura, K., Stocker, T.F., 2008. High-resolution carbon dioxide concentration record 650,000–800,000 years before present. Nature 453, 379–382.
Maher, B.A., Thompson, R., 1991. Mineral magnetic record of the Chinese loess and palaeosols. Geology 19, 3–6.
Marković, S.B., Hambach, U., Catto, N., Jovanović, M., Buggle, B., Machalett, B., Zöller, L., Glaser, B., Frechen, M., 2009. Middle and late Pleistocene loess sequences at Batajnica, Vojvodina, Serbia. Quat. Int. 198, 255–266.
Marković, S.B., Hambach, U., Stevens, T., Jovanoviä, M., O'Hara-Dhand, K., Basarin, B., Lu, H.Y., Smalley, I., Buggle, B., Zech, M., Svirčev, Z., Sümegi, P., Milojković, N., Zöller, L., 2012. Loess in the Vojvodina region (northern Serbia): an essential link between European and Asian Pleistocene environments. Neth. J. Geosci. 91, 173–188.
Marković, S.B., Stevens, T., Kukla, G.J., Hambach, U., Fitzsimmons, K.E., Gibbard, P., Buggle, B., Zech, M., Guo, Z.T., Hao, Q.Z., Wu, H.B., O'Hara Dhand, K., Smalley, I., Újvári, G., Sümegi, P., Timar-Gabor, A., Veres, D., Sirocko, F., Jary, Z., Svensson, A., Jović, V., Kovács, J., Zvirčev, Z., Vasiljević, D.A., 2015. Danube loess stratigraphy towards a pan-European loess stratigraphic model. Earth Sci. Rev. 148, 228–258.
Meng, X.Q., Liu, L.W., Wang, X.C.T., Balsam, W., Chen, J., Ji, J.F., 2018. Mineralogical evidence of reduced East Asian summer monsoon rainfall on the Chinese loess plateau during the early Pleistocene interglacials. Earth Planet. Sci. Lett. 486, 61–69.
Muri, H., Berger, A., Yin, Q.Z., Voldoire, A., Salas, D., Sundaram, S., 2012. SST and ice sheet impacts on the MIS-13 climate. Clim. Dyn. 39, 1739–1761. https://doi.org/10.1007/s00382-011-1216-9.
Muri, H., Berger, A., Yin, Q.Z., Karami, M.P., Barriat, P.Y., 2013. The climate of the MIS-13 interglacial according to HadCM3. J. Clim. 26, 9696–9712.
Peng, S.S., Ge, J.Y., Li, C.Z., Liu, Z.X., Qi, L., Tan, Y.L., Cheng, Y., Deng, C.L., Qiao, Y.S., 2015. Pronounced changes in atmospheric circulation and dust source area during the mid-Pleistocene as indicated by the Caotan loess-soil sequence in North China. Quat. Int. 372, 97–107.
Pisias, N.G., Rea, D.K., 1988. Late Pleistocene paleoclimatology of the central equatorial Pacific: sea surface response to the southeast trade winds. Paleoceanography 3, 21–37.
Porter, S.C., An, Z.S., 1995. Correlation between climate events in the north Atlantic and China during the last glaciation. Nature 375, 305–308.
Qian, W., Lin, X., Zhu, Y., Xu, Y., Fu, J., 2007. Climatic regime shift and decadal anomalous events in China. Clim. Change 84, 167–189.
Qiao, Y.S., Zhao, Z.Z., Wang, Y., Fu, J.L., Wang, S.B., Jiang, F.C., 2010. Variations of geochemical compositions and the paleoclimatic significance of a loess-soil sequence from Ganzi county of western Sichuan Province, China. Chin. Sci. Bull. 55, 255–260 (in Chinese).
Rossignol-Strick, M., Paterne, M., Bassinot, F.C., Emeis, K.C., De Lange, G.J., 1998. An unusual mid-Pleistocene monsoon period over Africa and Asia. Nature 392, 269–272.
Shi, P.H., Yang, T.B., Tian, Q.C., Jiang, S., Fan, Z., Wang, J.Y., 2013. Loess record of climatic changes during MIS 12–10 in the Jingyuan section, northwestern Chinese Loess Plateau. Quat. Int. 296, 149–159.
Sui, Y.Z., 2006. Study on environmental significant of main indexes of loess. J. Desert Res. 26, 15–19 (in Chinese with English abstract).
Sun, J.M., Ding, Z.L., Liu, T.S., Rokosh, D., Rutter, N., 1999. 580,000-year environmental reconstruction from aeolian deposits at the Mu Us Desert margin, China. Quat. Sci. Rev. 18, 1351–1364.
Sun, Y.B., Chen, J., Clemens, S.C., Liu, Q.S., Ji, J.F., Tada, R., 2006a. East Asian monsoon variability over the last seven glacial cycles recorded by a loess sequence from the northwestern Chinese Loess Plateau. Geochem. Geophys. Geosyst. 7, 97–112.
Sun, Y.B., Clemens, S.C., An, Z.S., Yu, Z.W., 2006b. Astronomical timescale and palaeoclimatic implication of stacked 3.6-Myr monsoon records from the Chinese Loess Plateau. Quat. Sci. Rev. 25, 33–48.
Sun, Y.B., Ma, L., Bloemendal, J., Clemens, S., Qiang, X.K., An, Z.S., 2015. Miocene climate change on the Chinese Loess Plateau: possible links to the growth of the northern Tibetan Plateau and global cooling. Geochem. Geophys. Geosyst. 16, 2097–2108.
Sundaram, S., Yin, Q.Z., Berger, A., Muri, H., 2012. Impact of ice sheet induced North Atlantic oscillation on East Asian summer monsoon during an interglacial 500,000 years ago. Clim. Dyn. 39, 1093–1105.
Tan, M., Nan, S.L., 2010. Primary investigation on interannual changes in the circulation effect of precipitation oxygen isotopes in monsoon China. Quat. Sci. 30, 620–622 (in Chinese with English abstract).
Tao, S.Y., Wei, J., 2006. The westward, northward advance of the subtropical high over the west Pacific in summer. J. Appl. Meteorol. Sci. 17, 514–525 (in Chinese with English abstract).
Vidic, N.J., TenPas, J.D., Verosub, K.L., Singer, M.J., 2000. Separation of pedogenic and lithogenic components of magnetic susceptibility in the Chinese loess/palaeosol sequence as determined by the CBD procedure and a mixing analysis. Geophys. J. Int. 142, 551–562.
Wang, B., Wu, R.G., Fu, X.H., 2000c. Pacific-East Asian teleconnection: how does ENSO affect East Asian climate? J. Clim. 13, 1517–1536.
Wang, P.X., Prell, W., Blum, P., 2000b. Exploring the Asian monsoon through drilling in the south China sea. Earth Sci. Front. 377.
Wang, S.B., Wu, X.H., Jiang, F.C., Tian, G.Q., Liu, K., 2000a. Two loess profiles in Pinglu, Shanxi and corresponding to paleoclimatic reconstruction. J. Geomech. 6, 28–36 (in Chinese with English abstract).
Wang, X.S., Yang, Z.Y., Løvli, R., Pei, J.L., Sun, Z.M., 2006. Environmental magnetism and paleoclimatic interpretation of the Sanmenxia loess-paleosol sequence in the southern extremity of the Chinese Loess Plateau. Chin. Sci. Bull. 55, 2755–2762 (in Chinese).
Webster, P.J., Magaña, V.O., Palmer, J., Shukla, R.A., Tomas, M., Tania, T., Yasunari, 1998. Monsoons: processes, predictability, and the prospects for prediction. J. Geophys. Res. 103, 14451–14510.
Wu, G.J., Pan, B.T., Li, J.J., Guan, Q.Y., Liu, Z.G., 2001. Tectonic-climatic events in eastern Qilian Mountains over the past 0.83 Ma. Sci. China Ser. D Earth Sci. D 44,

251–260.
Xiong, S.F., Ding, Z.L., Liu, T.S., 2001. Climatic implications of loess deposits from the Beijing region. J. Quat. Sci. 16, 575–582.
Xiong, S.F., Jiang, W.Y., Yang, S.L., Ding, Z.L., Liu, T.S., 2002. Northwestward decline of magnetic susceptibility for the red clay deposit in the Chinese loess plateau. Geophys. Res. Lett. 29, 15–1–15–4.
Xue, X.X., Yue, L.P., Zhou, J., Wang, J.Q., 2003. Susceptibility of the Late Cenozoic red earth–loess sequence in Xunyi, Shanxi province and environmental variation. Quat. Sci. 23, 104–108 (in Chinese with English abstract).
Yang, D., Fang, X.M., Song, Y.G., Li, J.J., An, Z.S., 2002. Pediment near the western Liupan mountain and its implication on the Neotectonic uplift. Acta Sedimentol. Sin. 20, 283–287 (in Chinese with English abstract).
Yang, D., Fang, X.M., Dong, G.R., Jin, J., Peng, Z.C., Li, J.J., 2006. Loess deposit characteristic in Duanxian section of Longxi basin and its reflected evolution of Tengger desert at north of China since last 1.8 Ma. J. Desert Res. 26, 7–13 (in Chinese with English abstract).
Yang, F., Lau, K.M., 2004. Trend and variability of China precipitation in spring and summer: linkage to sea–surface temperatures. Int. J. Climatol. 24, 1625–1644.
Yin, K., Hong, H.L., Churchman, G.J., Li, Z.H., Fang, Q., 2017. Mixed-layer illite-vermiculite as a paleoclimatic indicator in the Pleistocene red soil sediments in Jiujiang, southern China. Palaeogeogr. Palaeoclimatol. Palaeoecol. 510, 140–151.
Yin, Q.Z., Guo, Z.T., 2006. Mid-Pleistocene vermiculated red soils in southern China as an indication of unusually strengthened East Asian monsoon. Chin. Sci. Bull. 51, 213–220.
Yin, Q.Z., Guo, Z.T., 2008. Strong summer monsoon during the cool MIS-13. Clim. Past 4, 29–34.
Yin, Q.Z., Berger, A., Driesschaert, E., Goosse, H., Loutre, M.F., Crucifix, M., 2008. The Eurasian ice sheet reinforces the East Asian summer monsoon during the interglacial 500,000 years ago. Clim. Past 4, 79–90.
Yin, Q.Z., Berger, A., Crucifix, M., 2009. Individual and combined effects of ice sheets and precession on MIS-13 climate. Clim. Past 5, 229–243.
Yin, Q.Z., Berger, A., 2012. Individual contribution of insolation and CO_2, to the interglacial climates of the past 800,000 years. Clim. Dyn. 38, 709–724.
Yin, Q.Z., Singh, U.K., Berger, A., Guo, Z.T., Crucifix, M., 2014. Relative impact of insolation and the Indo-Pacific warm pool surface temperature on the East Asia summer monsoon during the MIS-13 interglacial. Clim. Past 10, 1645–1657.
Yu, Z., Wan, S., Colin, C., Yan, H., Bonneau, L., Liu, Z., Song, L., Sun, H., Xu, Z., Jiang, X., Li, A., Li, T., 2016. Co-evolution of monsoonal precipitation in East Asia and the tropical Pacific ENSO system since 2.36 Ma: new insights from high-resolution clay mineral records in the West Philippine Sea. Earth Planet. Sci. Lett. 446, 45–55.
Zhang, J., Li, J.J., Guo, B.H., Ma, Z.H., Li, X.M., Ye, X.Y., Yu, H., Liu, J., Yang, C., Zhang, S.D., Song, C.H., Hui, Z.C., 2016. Magnetostratigraphic age and monsoonal evolution recorded by the thickest quaternary loess deposit of the Lanzhou region, western Chinese loess plateau. Quat. Sci. Rev. 139, 17–29.
Zhang, W.G., Yu, L.Z., Lu, M., Zheng, X.M., Shi, Y.X., 2007a. Magnetic properties and geochemistry of the Xiashu Loess in the present subtropical area of China, and their implications for pedogenic intensity. Earth Planet. Sci. Lett. 260, 86–97.
Zhang, W.G., Yu, L.Z., Lu, M., Zheng, X.M., Ji, J.F., Zhou, L.M., Wang, X.Y., 2009. East Asian summer monsoon intensity inferred from iron oxide mineralogy in the Xiashu Loess in southern China. Quat. Sci. Rev. 28, 345–353.
Zhang, Y.G., Ji, J., Balsam, W.L., Liu, L., Chen, J., 2007b. High resolution hematite and goethite records from ODP 1143, South China Sea: co-evolution of monsoonal precipitation and El Niño over the past 600,000 years. Earth Planet. Sci. Lett. 264, 136–150.
Zhou, L.P., Oldfield, F., Wintle, A.G., Robinson, S.G., Wang, J.T., 1990. Partly pedogenic origin of magnetic variations in Chinese loess. Nature 346, 737–739.
Zhou, T.J., Yu, R.-C., 2005. Atmospheric water vapor transport associated with typical anomalous summer rainfall patterns in China. J. Geophys. Res. 110, D08104.
Zhou, W.J., Donahue, D.J., Porter, S.C., Jull, T.A., Li, X.Q., Stuiver, M., An, Z.S., Matsumoto, E., Dong, G.R., 1996. Variability of monsoon climate in East Asia at the end of the last glaciation. Quat. Res. 46, 219–229.
Zhu, N.N., Pan, B.T., Wang, J.P., Hu, Z.B., Su, H., Zhou, T., Hu, X.F., 2008. Grain size abrupt shift around 0.9 Ma in loess its environmental effect in Fenwei Basin, China. J. Desert Res. 2008 (28), 51–56 (in Chinese with English abstract).